

Theory of a one-atom laser in a photonic band-gap microchip

Lucia Florescu, Sajeev John, Tran Quang, and Rongzhou Wang

Department of Physics, University of Toronto, 60 St. George Street, Toronto, Ontario, Canada M5S 1A7

(Received 28 September 2003; published 26 January 2004)

We present a quantum theory of a coherently pumped two-level atom in a photonic band gap (PBG), coupled to both a multimode waveguide channel and a high-quality microcavity embedded within a photonic crystal. One mode is engineered to exhibit a sharp cutoff within the PBG, leading to a large discontinuity in the local photon density of states near the atom, and the cavity field mode is resonant with the central component of the Mollow spectrum of atomic resonance fluorescence. Another mode of the waveguide channel is used to propagate the pump beam. We derive analytical expressions for the optical amplitude, intensity, second-order correlation functions, and conjugate quadrature variances for the light emitted by the atom into the microcavity. The quantum degree of second-order coherence in the cavity field reveals enhanced, inversionless, nearly coherent light generation when the photon density of states jump between the Mollow spectral components is large. The cavity field characteristics are highly distinct from that of a corresponding high- Q cavity in ordinary vacuum. In the case of a vanishing photon density of states on the lower Mollow sideband and no dipolar dephasing, the emitted photon statistics is Poissonian, and the cavity field exhibits quadrature coherence.

DOI: 10.1103/PhysRevA.69.013816

PACS number(s): 42.55.Tv, 42.50.-p

I. INTRODUCTION

Photonic crystals (PCs) are periodic dielectric structures which can prohibit light propagation over a continuous range of frequencies, irrespective of the direction of propagation. The possibility of achieving photon localization [1] and photonic band gaps (PBGs) [2,3] has been a driving force behind the synthesis of these microstructures. This, in turn, has provided a compelling starting point for research of both fundamental and technological importance.

One of the key features that distinguishes the photonic radiation reservoir associated with a PBG material from its free space counterpart is that the photonic density of states (DOS) within or near the PBG can nearly vanish or exhibit discontinuous changes as a function of frequency with appropriate engineering. This leads to interesting optical phenomena, such as photon-atom bound states [4], fractionalized single-atom inversion [5], optical bistability and switching in multiatom systems [6], possible modification of Planck black-body radiation in microstructured metals [7], and coherent control of spontaneous emission through quantum interference [8].

Recent advances in the fabrication of photonic crystals [9] have been accompanied by studies of lasing in these materials [10]. On the other hand, a microlaser with a single atom or a quantum dot interacting with the quantized field of a high- Q microcavity represents a unique tool for the investigation of quantum electrodynamic effects. In free space, in the optical domain, high- Q optical cavities have allowed investigations of the vacuum Rabi splitting [11], photon antibunching [12], and conditional phase shifts for quantum logic gates [13]. In addition, the realization of an optical laser containing only a single active atom has been reported [14]. In such a system, it is possible to study the lasing process at the quantum level and identify features not readily distinguished in conventional laser systems. The one-atom laser theory in free space [15,16] has been developed for the case of weak coupling, in which the loss rate γ associated

with the spontaneous emission and cavity decay rate κ are much larger than the atom-cavity (coupling) frequency scale g , describing reversible evolution in the interaction of the atom with the cavity mode. The theory of the free space, one-atom laser with strong coupling has been developed [17–19] mainly by numerical means.

In this paper we present a detailed quantum theory of the unique features of a one-atom laser in an engineered PBG microchip. We study the effect of coherent pumping near a discontinuous photonic DOS on the quantum features of laser emission. Using a secular approximation [20], our model yields an analytical solution for the emission intensity and coherence properties. In particular, we demonstrate strong enhancement of the cavity field (relative to free space) and enhanced coherence, resulting from the radiation reservoir of the PBG microchip. We also present a specific photonic crystal architecture for the practical realization of this system. This consists of a quantum dot embedded in a dielectric microcavity placed within a multimode waveguide channel in a PBG microchip.

The outline of this paper is as follows. In Sec. II, we present the photonic crystal architecture relevant for the system we study. In Sec. III, we present the model Hamiltonian and derive the master equation for the atom-cavity system within coherent pumping. In Sec. IV, we investigate the effect of the magnitude of the photonic DOS discontinuity and microcavity quality factor on the emission amplitude and intensity. The coherence properties of the emission are derived in Sec. V. Finally, in Sec. VI, we discuss the results and possible generalizations of the model developed here.

II. PHOTONIC CRYSTAL ARCHITECTURE FOR A ONE-ATOM MICROLASER

We begin by demonstrating how photonic crystal (defect mode) engineering can be used to physically realize the model Hamiltonian we present in this paper for the one-atom laser. The fundamental challenge is to obtain strong coupling

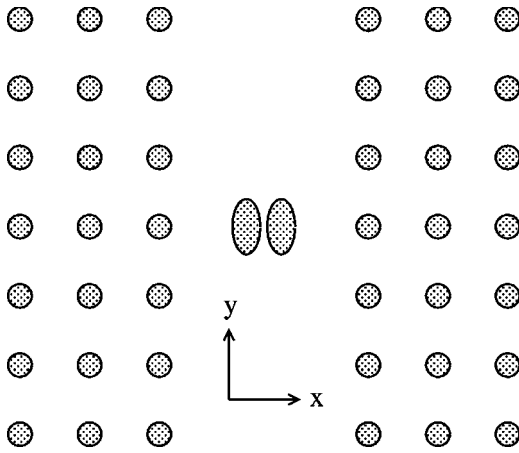


FIG. 1. The configuration of the hybrid structure. Two lines of rods (parallel to the y axis) are removed from the 2D photonic crystal to form a two-mode waveguide. In the center of the waveguide, two identical elliptic rods are introduced as defect rods. The major axes of these two elliptic rods are parallel to the waveguide direction. The semimajor axis is $r_y = 0.4a$ and the semiminor axis is $r_x = 0.2a$. The distance between two elliptic rods (from center to center) is $0.5a$.

within the PBG of the atom with an external pump laser and a high-quality-factor microcavity. While the first condition can be satisfied by replacing the atom (Q dot) within the waveguide channel of a three-dimensional (3D) PBG material, strong coupling of the atom to a microcavity requires that the microcavity is also in close proximity to the waveguide. In general, this may lead also to direct, strong coupling between the microcavity and the waveguide, with a concomitant degradation of the Q factor of the microcavity. In our photonic crystal architecture, we overcome this problem by designing the symmetry of the electromagnetic modes of the waveguide and the microcavity, so that this direct coupling is eliminated by orthogonality. In this way, both the atom-microcavity coupling and the atom-waveguide coupling can be strong, whereas the direct microcavity-waveguide coupling is suppressed. In order to achieve a factor of 100 jump in the reservoir density of states, a three-dimensional PBG architecture is useful. A general technique for embedding the waveguides and microcavity in a 3D PBG material using an intercalated two-dimensional microchip layer has been presented elsewhere [21]. For simplicity of illustration, we consider below a purely 2D photonic crystal with the understanding that the 2D architecture is embedded in a 2D-3D heterostructure [21].

In Fig. 1, we depict the top view of a 2D microchip layer that is sandwiched between suitable 3D PBG cladding layers above and below. The 2D microchip consists of a square lattice of cylindrical dielectric rods in an air background. Two missing rows of these rods represent a two-mode waveguide channel. The rods with elliptical cross section within this waveguide channel represent a microcavity resonator. We consider a quantum dot embedded within one of these elliptical defect rods. There are two kinds of electromagnetic modes in 2D photonic crystals. One is the E -polarization mode, i.e., the electric field is parallel to the rods. The other

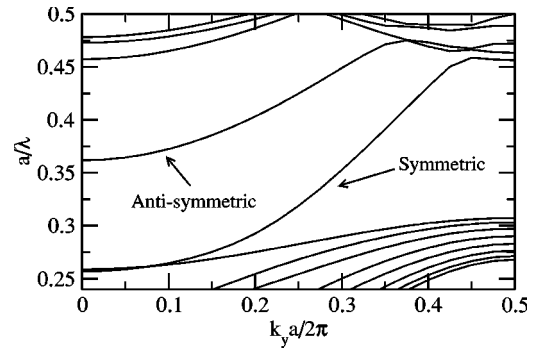


FIG. 2. The band structure of the waveguide structure formed by removing two lines of rods from the 2D photonic crystal, which has a band gap in the range $(0.308-0.453) 2\pi c/a$. Inside the band gap, the lower waveguide mode is symmetric about the center line of the waveguide, while the higher waveguide mode is antisymmetric.

is the H -polarization mode, where the magnetic field is parallel to the rods. For simplicity, only the E -polarization mode is considered here. Both the plane wave expansion method [22] and the supercell method [23] are used to calculate the band structure and the electric field pattern of the relevant modes. A 2D photonic crystal with a square lattice (lattice constant a) and circular dielectric rods (radius $r_0 = 0.17a$) is used. The dielectric constant of the rods is 11.9. This structure has a band gap in the range $(0.308-0.453) 2\pi c/a$. In our expansion, plane wave wave vectors are chosen by the condition $|\mathbf{G}| \leq 4.0(2\pi/a)$, where $|\mathbf{G}|$ is a reciprocal lattice vector.

When one line of rods is removed from the 2D photonic crystal, a waveguide is formed with its mode frequency inside the photonic band gap [24]. Usually, this waveguide mode is a symmetric mode, i.e., the electric field pattern has a mirror symmetry about the axis (center line) of propagation. If two lines of rods are removed, there are two waveguide modes inside the band gap. One mode is symmetric and the other is antisymmetric with respect to the waveguide axis (see Fig. 2). The antisymmetric mode usually has higher energy than the symmetric one because the antisymmetric mode has one node in the field pattern while the symmetric one has none. The field pattern of symmetric and antisymmetric waveguide modes (for the E -polarized modes of the 2D photonic crystal depicted in Fig. 1) is plotted in Fig. 3. In

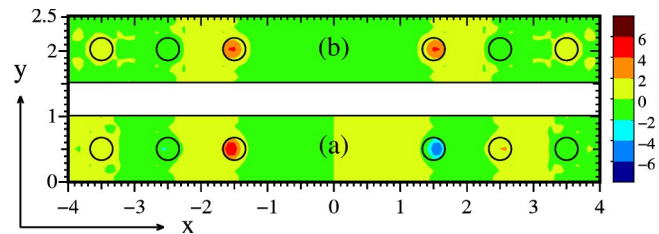


FIG. 3. The field patterns of waveguide modes. The x and y axes are in units of lattice constant a . The solid lines are dielectric rods. (a) The real part of the electric field of the symmetric waveguide mode when $k_y = 0.3(2\pi/a)$; (b) the imaginary part of the electric field of the antisymmetric waveguide mode when $k_y = 0$. The direction of propagation is along the y axis.

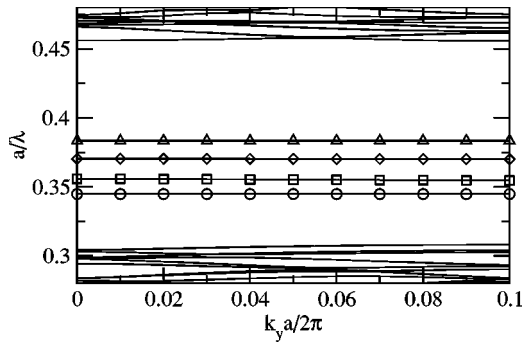


FIG. 4. The band structure of the defect structure formed by changing two nearby rods of the 2D photonic crystal into larger rods. The radius of the defect rods is $0.3a$, where a is the square lattice constant. The solid lines with various symbols are defect modes.

the calculations of the waveguide modes, the supercell contains 10×1 unit cells of the square lattice, where the x axis is normal to the waveguide direction and the y axis is in the waveguide direction.

Near the cutoff frequency of the antisymmetric mode, the local electromagnetic density of states (LDOS) in the vicinity of the waveguide channel exhibits a peak whose height is limited by the overall length (in the y direction) of the sample. For an infinite system, this LDOS becomes a square-root singularity. In addition to this peak, the LDOS has a small background contribution from the symmetric mode, which has a large group velocity and nearly linear dispersion near the cutoff frequency of the antisymmetric mode. We now describe the introduction of an additional microcavity defect near the waveguide, with an isolated, localized mode of frequency near the waveguide cutoff.

If only one single rod (instead of one line of rods) is removed or changed, a localized defect mode (microcavity mode) can be created within the PBG [25]. When the rod is replaced by a rod larger than the original ones (dielectric defect), two degenerate modes can be created. The localized electric field pattern has a dipolar character, and these two degenerate modes correspond to dipoles along two perpendicular directions (denoted \uparrow and \rightarrow). These defect modes form sharp peaks (of width inversely proportional to their Q factor) in the LDOS. However, the naive introduction of a defect near our waveguide structure will, in general, disrupt the band structure of the waveguide mode, due to direct coupling between modes with the same symmetry. Since the dipole mode \uparrow is symmetric, it will strongly couple to the symmetric waveguide mode, leading to rapid decay of radiation (low Q) from the microcavity. To avoid direct coupling between the waveguide mode and the microcavity mode, we can engineer the defect rods to support only one antisymmetric localized mode inside the band gap. This is realized below by introducing two defect rods of suitable shape.

In general, if two neighboring rods are replaced by larger defect rods in a 2D photonic crystal, four defect modes will be formed in the band gap (Fig. 4). These two defect rods have the same radius $r=0.3a$; and the supercell has 10×4 unit cells of the square lattice. The electric field pattern of these defect modes is plotted in Fig. 5. These modes are

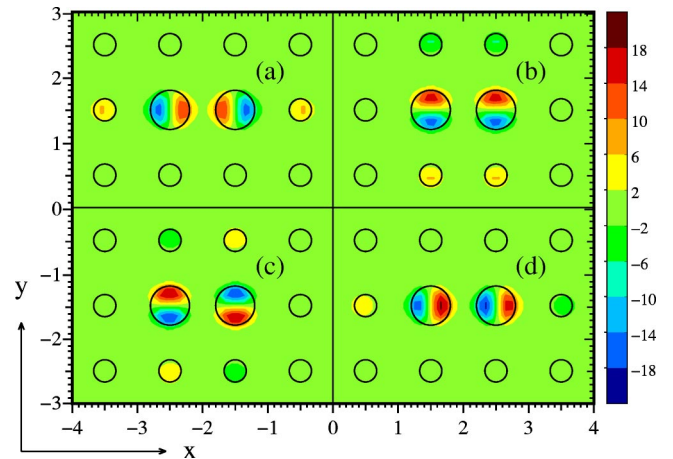


FIG. 5. The electric field pattern of the defect modes when $k = 0$. The solid lines are dielectric rods. (a) The $\rightarrow\leftarrow$ mode; (b) the $\uparrow\uparrow$ mode; (c) the $\uparrow\downarrow$ mode; and (d) the $\leftarrow\leftarrow$ mode.

composed of two dipole patterns arranged in the following way (frequencies from low to high): $\rightarrow\leftarrow$, $\uparrow\uparrow$, $\uparrow\downarrow$, and $\leftarrow\leftarrow$. Among these four defect modes, the mode with field pattern $\uparrow\downarrow$ can provide a high- Q cavity mode if centered on the waveguide axis. This mode is antisymmetric about the axis of the waveguide, so it will not couple to the symmetric waveguide mode. Moreover, this mode is antisymmetric about the line connecting the rod centers. Therefore, it also is orthogonal to the antisymmetric waveguide mode (at $k_y = 0$) if the line connecting the rod centers is perpendicular to the waveguide direction. As a result, this mode can be brought to the vicinity of the cutoff frequency of the antisymmetric waveguide mode (which occurs at $k_y = 0$) without disturbing the LDOS discontinuity.

In order to remove spurious defect modes from the band gap, both the shape and the position of the defect rods can be engineered. Using elliptic defect rods, in place of circular defect rods, selects modes with dipole along the major axis of the ellipse. For sufficient ellipticity, two modes with dipole along the minor axis can be removed from the band gap. In this case, only two modes with electric field pattern $\uparrow\uparrow$ and $\uparrow\downarrow$ remain in the PBG. To further separate these remaining defect modes, the distance between the elliptic rods can be reduced. At an appropriate separation, only the desired $\uparrow\downarrow$ defect mode remains inside the bandgap.

The desired microlaser architecture is shown in Fig. 1. Two columns of rods are removed from the 2D photonic crystal to form a waveguide and two identical elliptic rods are placed on either side of the waveguide axis (within the waveguide). The major axes of these two elliptic rods are parallel to each other, as well as parallel to the waveguide direction. The semimajor axis is r_y and the semiminor axis is r_x , with $r_y:r_x=2:1$. The distance between the centers of the two defect rods is chosen to be $0.1a+2r_x$. When the semiminor axis r_x is around $0.2a$, only one defect mode is inside the band gap, and this mode is near the cutoff frequency of the antisymmetric waveguide mode.

In Fig. 6, the band structure of the system containing both waveguide and microcavity is plotted. The size of the defect rods decreases in Fig. 6(a) to Fig. 6(c) from $r_x=0.199a$ to

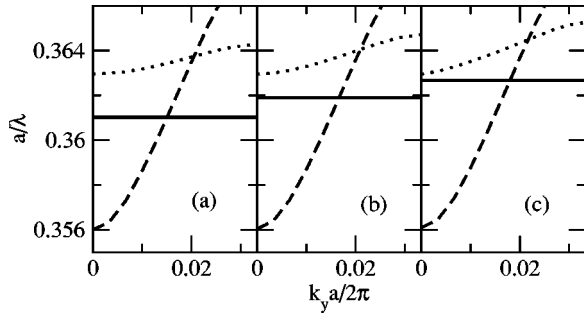


FIG. 6. The band structure of the one-atom, PBG laser with both waveguide and microcavity. The solid lines indicate the frequency of the cavity modes when $\mathbf{k}=\mathbf{0}$. The dashed lines are symmetric waveguide modes, and the dotted lines are antisymmetric waveguide modes. (a) The semiminor axis $r_x=0.199a$; (b) the semiminor axis $r_x=0.198a$; and (c) the semiminor axis $r_x=0.197a$.

$r_x=0.197a$. The supercell contains 10×15 unit cells of the square lattice. The symmetric waveguide mode goes from $0.356(2\pi c/a)$ (at $k_y=0$) to $0.368(2\pi c/a)$ [at $k_y=0.033(2\pi/a)$]. The antisymmetric waveguide mode goes from $0.363(2\pi c/a)$ (at $k_y=0$) to $0.3642(2\pi c/a)$ [at $k_y=0.033(2\pi/a)$]. The remaining mode is the microcavity mode whose frequency varies with the size of the defect rods. When $r_x=0.197a$, the microcavity mode frequency is very close to that of the cutoff frequency of the antisymmetric waveguide mode. However, as a result of symmetries of each mode, the microcavity does not couple directly to either

waveguide mode and retains a high Q factor.

The electric field patterns of both the cavity mode and the antisymmetric waveguide mode [with parameters corresponding to Fig. 6(c)] are plotted in Fig. 7. The electric field of the cavity mode is localized around the defect; while the waveguide mode spreads over the waveguide with some fields concentrated on the center of defect rods. The Q dot can be placed in one of the elliptical defect rods, where it couples strongly to both the waveguide mode and the cavity mode. We now consider a model Hamiltonian for atom-radiation field interactions near this microcavity in the frequency range of the antisymmetric waveguide mode cutoff.

III. DRESSED-STATE MASTER EQUATION

We consider a single two-level atom (quantum dot) strongly coupled to a high- Q microcavity described above and driven by a coherent external laser field propagating through the symmetric waveguide mode. The excited atomic system decays by spontaneous emission to the modes of the radiation reservoir (in our case, the waveguide modes) associated with the engineered photonic crystal. The atom has excited state $|2\rangle$, ground state $|1\rangle$, and transition frequency ω_a . The coupling constant between the atomic transition and the microcavity mode is denoted by g . The atom is driven near resonance by a coherent external field at a frequency ω_L and Rabi frequency (intensity) ε . The Rabi frequency characterizes the strength of the driving field, and is proportional to the product of the transition dipole moment d_{12} and the

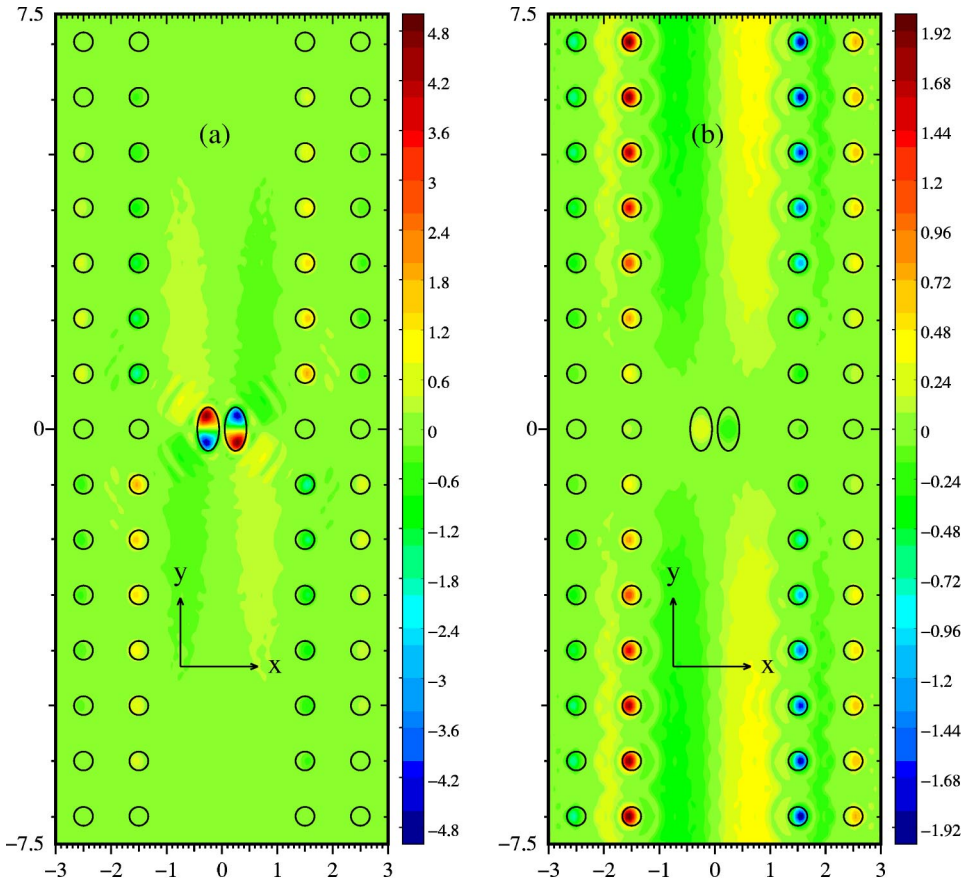


FIG. 7. The electric field pattern of the one-atom, PBG laser with both waveguide and microcavity. The parameters are the same as those in Fig. 6(c). The wave vector $\mathbf{k}=\mathbf{0}$. (a) The cavity mode and (b) the waveguide mode.

driving field amplitude E ($\varepsilon = d_{12}|E|/\hbar$). For simplicity, we treat the driving external field classically. The Hamiltonian of the system in the interaction picture is [26]

$$H = H_0 + H_1 + H_{dephase} + H_{damping}. \quad (3.1)$$

Here,

$$H_0 = \hbar \Delta_c a^\dagger a + \frac{1}{2} \hbar \Delta_a \sigma_3 + \hbar \varepsilon (\sigma_{12} + \sigma_{21}) + \hbar \sum_\lambda \Delta_\lambda a_\lambda^\dagger a_\lambda, \quad (3.2)$$

and the individual terms (in the order they appear) describe the unperturbed microcavity field, the atomic system, the interaction between the atomic system and the monochromatic pump laser field, and the remainder of the radiation reservoir of the photonic crystal (responsible for the radiative decay of the atom). In our case, this reservoir consists of the waveguide modes within the PBG. The interaction Hamiltonian is

$$H_1 = i\hbar g (a^\dagger \sigma_{12} - \sigma_{21} a) + i\hbar \sum_\lambda g_\lambda (a_\lambda^\dagger \sigma_{12} - \sigma_{21} a_\lambda). \quad (3.3)$$

The individual terms (in the order they appear) describe the interaction between the atomic system and the microcavity field, and the interaction between the atomic system and the remainder of the photonic crystal radiation reservoir. Here, a and a^\dagger are the cavity-mode annihilation and creation operators. σ_{ij} are the bare atomic operators, $\sigma_{ij} = |i\rangle\langle j|$ ($i, j = 1, 2$), and $\sigma_3 = \sigma_{22} - \sigma_{11}$ describes the bare atomic inversion. The coupling constant between the atom and the cavity mode is given by $g = (\omega_a d_{21}/\hbar)(\hbar/2\varepsilon_0 \omega_c V)^{1/2} \mathbf{e} \cdot \mathbf{u}_d$, where d_{12} and \mathbf{u}_d are the absolute value and the unit vector of the atomic dipole moment, V is the volume of the cavity mode, \mathbf{e} is the polarization mode of the cavity radiation field, and ε_0 is the dielectric constant. In the optical regime, dipole moments of [27] $d_{21} \approx 10^{-29}$ C m, and a microcavity mode volume of $V \approx (1 \mu\text{m})^3$ yield $g \approx 10^{-5} \omega_a$. a_λ and a_λ^\dagger are the photonic crystal radiation reservoir annihilation and creation operators. $\Delta_a = \omega_a - \omega_L$, $\Delta_c = \omega_c - \omega_L$, and $\Delta_\lambda = \omega_\lambda - \omega_L$, are the detuning of the atomic resonance frequency ω_a , of the cavity-mode frequency ω_c , and of the frequency ω_λ of a mode λ of the photonic crystal radiation reservoir. g_λ is the coupling constant between the atom and the mode λ of the radiation field of the photonic reservoir. The relevant frequencies for our study, and their relative position are presented in Fig. 8.

One of the unique features of the quantum electrodynamics (QED) in a photonic crystal is the possibility to simultaneously realize extremely small microcavity mode volumes and maintain very high cavity Q factors. For instance, in a 2D photonic crystal, a microlaser with a cavity volume of $0.03 \mu\text{m}^3$ has already been demonstrated [28]. Within a 3D PBG, with complete light localization [1,3], there is no fundamental upper bound to the microcavity Q factor. In our case, the Q factor is determined by the degree of coupling to the engineered waveguide modes within the PBG and possible leakage of light from the microcavity in the vertical direction (surface emitting laser).

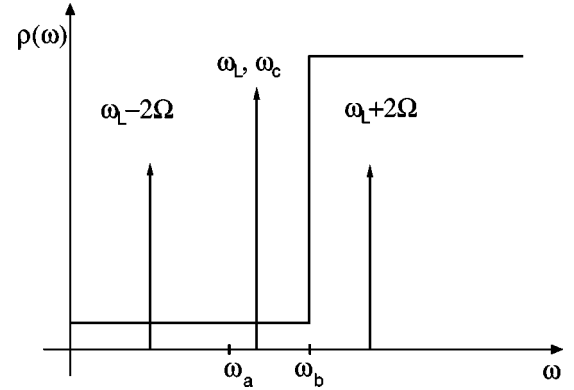


FIG. 8. The relative positions of the relevant frequencies considered in our study. ω_a , ω_L , and ω_c are the atomic transition frequency, the frequency of the coherent pump field, and the microcavity field frequency, respectively. $\omega \pm 2\Omega$ describe the sideband components of the Mollow spectrum (Ω is the generalized Rabi frequency), and ω_b is the photonic DOS band edge frequency.

The Hamiltonian $H_{dephase}$ describes additional dephasing interactions, which may arise from atomic collisions and scattering of phonons from the impurity atoms, if the atom is embedded in the solid part of the dielectric material. We assume for simplicity that the phonon DOS is broad and displays no sharp features. In this case, the dephasing part of the master equation for the density operator χ of the atom-cavity-reservoir system can be written as [29]

$$\left(\frac{\partial \chi}{\partial t} \right)_{dephase} = \gamma_p (\sigma_3 \chi \sigma_3 - \chi), \quad (3.4)$$

where γ_p is a phenomenological dephasing rate.

The Hamiltonian $H_{damping}$ describes the damping of the cavity field. In our case, this may arise from infinitesimal asymmetry of the defect architecture or disorder in the waveguide channel (caused by the manufacturing process) that allow weak direct coupling between the waveguide mode and the microcavity mode within the PBG. Also, a small amount of light can be emitted in the vertical (z direction) by making the thickness of the 3D PBG cladding layers smaller in the vicinity of the microcavity. The contribution of this type of damping to the master equation is expressed as

$$\left(\frac{\partial \chi}{\partial t} \right)_{damping} = \frac{\kappa}{2} [2a\rho a^\dagger - a^\dagger a \chi - \rho a^\dagger a]. \quad (3.5)$$

Here, κ is the phenomenological cavity decay rate. The cavity quality factor is then defined as $Q \equiv \omega/\kappa$.

The radiative part of the master equation for the density operator χ of the system has the form

$$\left(\frac{\partial \chi}{\partial t} \right)_{rad} = \frac{i}{\hbar} [H, \chi]. \quad (3.6)$$

Equation (3.4) is written in the basis $\{|i\rangle\}_{i=1,2}$, of bare atomic states. It is useful to use the dressed-state picture, by introducing the states $\{|\tilde{i}\rangle\}_{i=1,2}$ [6,18] of the atomic system dressed by the driving field,

$$|\tilde{1}\rangle = c|1\rangle - s|2\rangle, \quad (3.7)$$

$$|\tilde{2}\rangle = s|1\rangle - c|2\rangle. \quad (3.8)$$

Here, $c \equiv \cos(\phi)$, $s \equiv \sin(\phi)$, and ϕ is the rotation angle, which belongs in the interval $[0, \pi]$ and is defined by

$$\cos^2 \phi = \frac{1}{2} \left(1 + \frac{\Delta_a}{\Omega} \right), \quad (3.9)$$

and

$$\Omega = (4\epsilon^2 + \Delta_a^2)^{1/2}, \quad (3.10)$$

is the generalized Rabi frequency.

The atom-applied field part of the Hamiltonian H_0 can be diagonalized using the transformation

$$\sigma_{12} = \frac{1}{2} \sin(2\phi) R_3 - \sin^2 \phi R_{21} + \cos^2 \phi R_{12}, \quad (3.11a)$$

$$\sigma_{22} - \sigma_{11} = \cos(2\phi) R_3 - \sin(2\phi) (R_{12} + R_{21}), \quad (3.11b)$$

$$R_3 = R_{22} - R_{11}, \quad (3.11c)$$

where $R_{ij} = |\tilde{i}\rangle\langle\tilde{j}|$ are the dressed-state atomic operators. This leads to the dressed-state Hamiltonian

$$H_0 = \hbar\Omega R_3 + \hbar\Delta_c a^\dagger a + \hbar \sum_{\lambda} \Delta_{\lambda} a_{\lambda}^{\dagger} a_{\lambda}. \quad (3.12)$$

In the dressed-state basis, the bare atomic operators σ_{12} , σ_{21} , and σ_3 in the interaction Hamiltonian, H_1 , and $(\partial\chi/\partial t)_{dephase}$ are replaced by the expressions (3.11a) and (3.11b). Further, we define the time-dependent interaction picture Hamiltonian $\tilde{H}_1(t) = U^\dagger(t) H_1 U(t)$, where $U(t) = \exp(-iH_0 t/\hbar)$. In this interaction picture, the interaction Hamiltonian takes the form

$$\begin{aligned} H_1 = & i\hbar g (s c a^\dagger R_3 e^{i\Delta_c t} + c^2 a^\dagger R_{12} e^{i(\Delta_c - 2\Omega)t} \\ & - s^2 a^\dagger R_{21} e^{i(\Delta_c + 2\Omega)t}) + i\hbar \sum_{\lambda} g_{\lambda} (s c a_{\lambda}^{\dagger} R_3 e^{i\Delta_{\lambda} t} \\ & + c^2 a_{\lambda}^{\dagger} R_{12} e^{i(\Delta_{\lambda} - 2\Omega)t} - s^2 a_{\lambda}^{\dagger} R_{21} e^{i(\Delta_{\lambda} + 2\Omega)t}) + \text{H.c.} \end{aligned} \quad (3.13)$$

Here and below, we drop the tilde on the interaction picture operators, for the sake of notational simplicity.

The interaction-picture density operator χ obeys a master equation whose radiative part is similar to Eq. (3.6), where the total Hamiltonian H is replaced by the interaction-picture Hamiltonian H_1 . This equation is formally integrated, and the solution is replaced into the right-hand side of the equation. Further, the master equation for the reduced density operator of the system of atom plus cavity, $\rho = \text{Tr}_R \chi$ (here, Tr_R denotes a trace over the reservoir variables), is obtained from the resulting master equation by tracing over the photonic crystal radiation reservoir variables [29]:

$$\left(\frac{\partial \rho}{\partial t} \right)_{rad} = - \frac{1}{\hbar^2} \int_0^t dt' \text{Tr}_R \{ [H_1(t), [H_1(t'), \chi(t')]] \}. \quad (3.14)$$

In the Born approximation [29], the operator $\chi(t')$ in Eq. (3.14) is replaced by $\rho(t') R_0$, where R_0 is an initial reservoir density operator. This corresponds to the second-order perturbation theory in the interaction between the atom and reservoir. It assumes that changes in the reservoir as a result of atom-reservoir interaction are negligible. Further, we assume that the photonic density of states at the atomic frequency exhibits a step discontinuity, so that the Mollow components of the fluorescent scattering spectrum [29,5] at frequencies ω_L , $\omega_L - 2\Omega$, and $\omega_L + 2\Omega$ experience strongly different mode densities. For simplicity, we assume that, while singular at one frequency, the photonic density of modes is constant over the spectral regions surrounding the dressed-state resonant frequencies ω_L , $\omega_L - 2\Omega$, and $\omega_L + 2\Omega$. This allows [29] for a Markovian treatment of the atom-radiation reservoir system. The Markovian approximation neglects memory effects and replaces $\rho(t')$ by $\rho(t)$. In the Born-Markov approximation, the master equation for the system atom-cavity field, obtained from Eqs. (3.14), (3.4), and (3.5), is

$$\begin{aligned} \frac{\partial \rho}{\partial t} = & g \{ s c [a^\dagger R_3 e^{i\Delta_c t} - R_3 a e^{-i\Delta_c t}, \rho] + c^2 [a^\dagger R_{12} e^{i(\Delta_c - 2\Omega)t} - R_{21} a e^{-i(\Delta_c - 2\Omega)t}, \rho] \\ & - s^2 [a^\dagger R_{21} e^{i(\Delta_c + 2\Omega)t} - R_{12} a e^{-i(\Delta_c + 2\Omega)t}, \rho] \} + \left\{ \frac{A_0}{2} [R_3 \rho R_3 - \rho] + \frac{A_-}{2} [R_{21} \rho R_{12} - R_{12} R_{21} \rho] \right. \\ & \left. + \frac{A_+}{2} [R_{12} \rho R_{21} - R_{21} R_{12} \rho] + \text{H.c.} \right\} + \frac{\kappa}{2} [2a \rho a^\dagger - a^\dagger a \rho - \rho a^\dagger a]. \end{aligned} \quad (3.15)$$

The first group of terms in the master equation (3.15) correspond to the interaction between the dressed atomic system and the cavity mode, the second group of terms describes the spontaneous emission of the dressed atom into the modes of the photonic crystal radiation reservoir, and the last group of terms describes the damping of the cavity mode via cavity

decay. Here, we assume that the cavity and the photonic reservoirs are independent [29]. In this case, the spontaneous emission is described by the same type of terms as in the case when no cavity is present in the system, derived in Ref. [6]. In Eq. (3.15), $A_0 = \gamma_0 s^2 c^2 + \gamma_p (c^2 - s^2)$, $A_- = \gamma_- s^4 + 4\gamma_p s^2 c^2$, and $A_+ = \gamma_+ c^4 + 4\gamma_p s^2 c^2$, and spontaneous emission decay rates $\gamma_0 = 2\pi \sum_\lambda g_\lambda^2 \delta(\omega_\lambda - \omega_L)$, $\gamma_- = 2\pi \sum_\lambda g_\lambda^2 \delta(\omega_\lambda - \omega_L + 2\Omega)$, and $\gamma_+ = 2\pi \sum_\lambda g_\lambda^2 \delta(\omega_\lambda - \omega_L - 2\Omega)$ are proportional to the density of modes at the dressed-state transition frequencies. In deriving the spontaneous emission terms in Eq. (3.15), we have used a secular approximation [20,6] valid for strong applied laser field or large detunings between the atomic and the laser frequencies. This approximation is based on the assumption that the generalized Rabi frequency Ω is much larger than the decay rates γ_0 , γ_+ , and γ_- ($\Omega \gg \gamma_0, \gamma_+, \gamma_-$), and consists in neglecting rapidly oscillating terms at frequencies 2Ω and 4Ω .

We focus our study on the case when the cavity field is tuned on resonance with the central component of the Mollow spectrum. Assuming $\Omega \gg \kappa$, we can use the secular approximation to ignore the rapidly oscillating terms at frequencies 2Ω and 4Ω in master equation (3.15). The master equation (3.15) reduces in this case to

$$\begin{aligned} \frac{\partial \rho}{\partial t} = & g_1 [(a^\dagger - a)R_3, \rho] + \left\{ \frac{A_0}{2} [R_3 \rho R_3 - \rho] + \frac{A_-}{2} [R_{21} \rho R_{12} \right. \\ & \left. - R_{12} R_{21} \rho] + \frac{A_+}{2} [R_{12} \rho R_{21} - R_{21} R_{12} \rho] + \text{H.c.} \right\} \\ & + \frac{\kappa}{2} [2a \rho a^\dagger - a^\dagger a \rho - \rho a^\dagger a]. \end{aligned} \quad (3.16)$$

Here, $g_1 \equiv gcs$ is the ‘‘effective’’ coupling constant.

In what follows, we employ the master equation (3.16) to derive the properties of the one-atom laser emission in the engineered vacuum of a PBG material.

IV. MICROCAVITY FIELD AMPLITUDE AND INTENSITY

In this section we investigate the influence of the properties of the engineered radiation reservoir on the emitted cavity field. The master equation (3.16) enables the derivation of equations of motion for expectation values of atomic and cavity field operators. These expectation values are defined as $\langle \dots \rangle = \text{Tr}(\rho \dots)$. Using the fact that $a, a^\dagger, R_{12}, R_{21}$, and R_3 are time-independent Schrödinger operators, the equations of motion for their expectation values follow from $\partial \rho / \partial t$ in the master equation (3.16). The following closed set of equations of motion for the expectation values of various operators is obtained:

$$\frac{d}{dt} \langle a \rangle = -\frac{\kappa}{2} \langle a \rangle + g_1 \langle R_3 \rangle, \quad (4.1a)$$

$$\frac{d}{dt} \langle R_3 \rangle = -\gamma_2 - \gamma_1 \langle R_3 \rangle, \quad (4.1b)$$

$$\frac{d}{dt} \langle a^\dagger a \rangle = -\kappa \langle a^\dagger a \rangle + g_1 \langle R_3 a^\dagger \rangle + g_1 \langle R_3 a \rangle, \quad (4.1c)$$

$$\frac{d}{dt} \langle R_3 a \rangle = -(\gamma_1 + \kappa/2) \langle R_3 a \rangle + g_1 - \gamma_2 \langle a \rangle, \quad (4.1d)$$

where $\gamma_{1,2}$ are defined by

$$\gamma_1 = \frac{\gamma_+ c^4 + \gamma_- s^4}{2} + 4\gamma_p s^2 c^2, \quad (4.2a)$$

$$\gamma_2 = \frac{\gamma_+ c^4 - \gamma_- s^4}{2}. \quad (4.2b)$$

In the steady-state regime, the dressed-state atomic population inversion $\langle R_3 \rangle_s$, the cavity field amplitude $\langle a \rangle_s$, and the mean number of photons $\langle a^\dagger a \rangle_s$ are obtained as

$$\langle R_3 \rangle_s = -\frac{\gamma_2}{\gamma_1}, \quad (4.3)$$

$$\langle a \rangle_s = \langle a^\dagger \rangle_s^* = -\frac{2g_1}{\kappa} \frac{\gamma_2}{\gamma_1}, \quad (4.4)$$

$$\langle a^\dagger a \rangle_s = \frac{4g_1^2}{\kappa^2} \frac{(\kappa\gamma_1 + 2\gamma_2)}{\gamma_1(\kappa + 2\gamma_1)}. \quad (4.5)$$

The properties of the cavity field can be studied using the expressions (4.4) and (4.5) for the cavity field amplitude $\langle a \rangle_s$ and the mean photon number $\langle a^\dagger a \rangle_s$. We note that light generation into the defect mode does not require positive bare atomic population inversion. In our model, the steady-state mean number of photons in the cavity field, $\langle a^\dagger a \rangle_s$, can be expressed in terms of the square of the bare atomic population inversion $\langle \sigma_3 \rangle_s$, rather than as a linear function of $\langle \sigma_3 \rangle_s$:

$$\langle a^\dagger a \rangle_s = \frac{4g_1^2}{\kappa^2(\kappa + 2\gamma_1)} \left[\kappa + \frac{\gamma^2 \gamma_1}{2\gamma_{2,0}^2} \langle \sigma_3 \rangle_s^2 \right]. \quad (4.6)$$

Here, we have used Eqs. (3.11b), and (4.1)–(4.5). γ is the spontaneous emission rate in free space, and $\gamma_{2,0} = (\gamma/2)(c^4 - s^4)$ is the free-space value of γ_2 . Clearly, strong intensity of the cavity field may be achieved for negative bare atomic population inversion, suggestive of inversionless light generation. We also note from expression (4.5) that the intensity of the cavity field increases with increasing g_1/κ and depends on the size of the discontinuity on the photonic density of states γ_-/γ_+ [see also Eq. (4.2)].

In Fig. 9, the steady-state cavity photon number $\langle a^\dagger a \rangle_s$ is plotted as a function of Rabi driving field frequency ε for various values of the magnitude of the discontinuity in the photonic density of states γ_-/γ_+ , ranging from the case of a full PBG with no waveguide mode for the lower Mollow sideband, $\gamma_-/\gamma_+ = 0$, to the free-space case, $\gamma_-/\gamma_+ = 1$, and no dipolar dephasing. We consider negative detuning between the atomic resonant frequency and the driving field

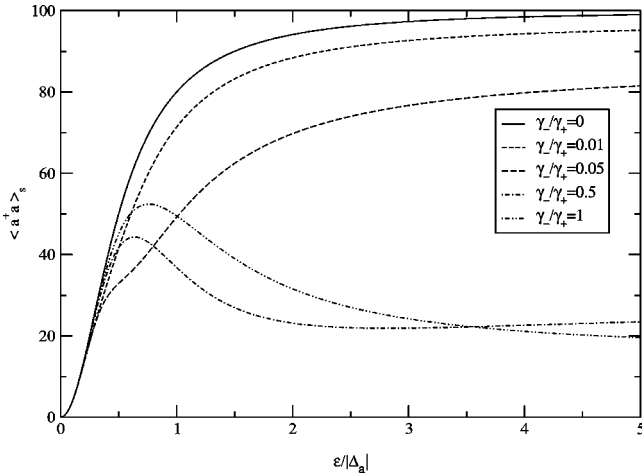


FIG. 9. The steady-state mean number of photons in the cavity $\langle a^\dagger a \rangle_s$ as a function of the scaled driving field Rabi frequency $\varepsilon/|\Delta_a|$, for negative detuning between the atomic resonant frequency and the driving field frequency $\Delta_a < 0$, in the absence of dipolar dephasing ($\gamma_p = 0$), and for various values of the jump in the photonic DOS γ_-/γ_+ . We have set $\kappa = 0.1\gamma_+$ and $g = 10\kappa$ in the calculations.

frequency $\Delta_a < 0$, a strong coupling regime $g/\kappa = 10$, and a cavity decay rate κ given by $\kappa/\gamma_+ = 0.1$. For a spontaneous emission decay rate $\gamma_+ = 100\gamma$, this cavity decay rate corresponds to a quality factor Q of 10^6 . For a frequency detuning $|\Delta_a| \approx 10^{-7}\omega$, in the optical regime, the values of the Rabi field frequency used in the calculations correspond to electric field amplitudes of $E \approx 10^3$ V/m. For a pump field passing through a waveguide channel of cross-sectional area $A \approx (1 \mu\text{m})^2$, this corresponds to nanowatts of power [30]. We note that the steady-state microcavity intensity as a function of the intensity of the coherent pump does not show a threshold behavior. It is essentially linearly amplified, as the driving field intensity increases. The absence of the threshold in the emission input-output characteristic is common in the quantum theory of one-atom lasers [17]. Our model, based on the assumption of a strong pumping field (but, actually, very low power, as shown above), is, strictly speaking, inapplicable in the threshold regime. In order to describe such a weak pumping regime, it is necessary to include non-Markovian dynamics in the atomic response [26]. We note from Fig. 9 that, above threshold, light generation is strongly enhanced in photonic structures presenting large jumps in the photonic density of states, relative to free space. For large values of the driving field intensity and large jumps in the photonic density of states, the mean number of photons in the cavity field exhibits saturation, corresponding to the saturation of the atomic population inversion [see Eq. (4.6)]. For smaller jumps in the photonic density of states, as well as in free space, the mean photon number decreases with further increase of the intensity of the driving field. These qualitative features can be explained by noting that the intensity emitted into the cavity mode by the dressed atomic system is determined by two factors: the effective coupling constant g_1 between the dressed atomic system and the cavity mode, and the absolute value of dressed-state population inversion

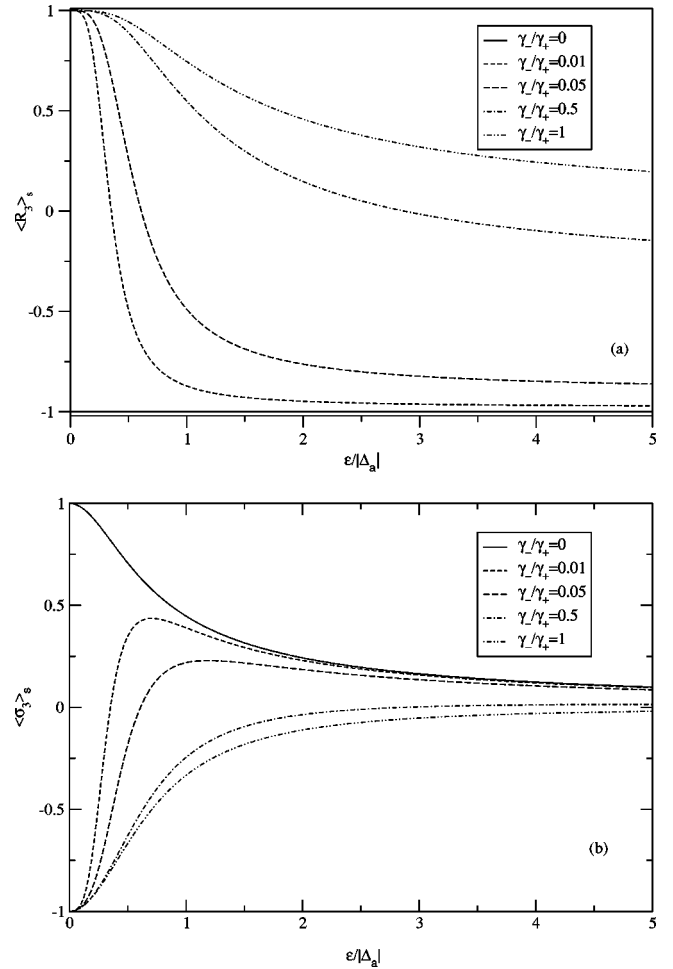


FIG. 10. The steady-state (a) dressed and (b) bare atomic population inversion $\langle R_3 \rangle_s$ and $\langle \sigma_3 \rangle_s$, as functions of the scaled driving field Rabi frequency $\varepsilon/|\Delta_a|$, for negative detuning between the atomic resonant frequency and the driving field frequency $\Delta_a < 0$, and for various values of the jump in the photonic DOS γ_-/γ_+ .

$|\langle R_3 \rangle|$ [see Eq. (4.1a)]. In free space, increasing $|\langle R_3 \rangle|$ leads to a decrease of g_1 [see Eqs. (4.3) and (4.2) and the definition of g_1]. On the other hand, in a photonic crystal, the jump in the photonic density of states facilitates the increase of $|\langle R_3 \rangle|$, without affecting the coupling constant. This, in turn, leads to the enhancement of the emission in photonic crystals. In Fig. 10, we plot the steady-state dressed-state and bare-state atomic population inversion, $\langle R_3 \rangle_s$ and $\langle \sigma_3 \rangle_s$ [given by Eq. (3.11b)], as functions of the driving field Rabi frequency, for the same values of the jump in the photonic DOS as for Fig. 9. We note that for large values of the jump in the photonic density of states of the radiation reservoir and at large driving field intensities, the dressed atomic system is trapped in the dressed ground state $|\tilde{1}\rangle$, and the dressed-state atomic population inversion achieves values close to -1 . This is accompanied by positive bare atomic population inversion. For smaller jumps in the photonic density of states, $\langle R_3 \rangle_s$ and $\langle \sigma_3 \rangle_s$ approach zero. The loss of light generation at large values of the driving field intensity for photonic structures with small jumps in the photonic DOS can be explained using Eq. (4.1a) for the cavity field amplitude

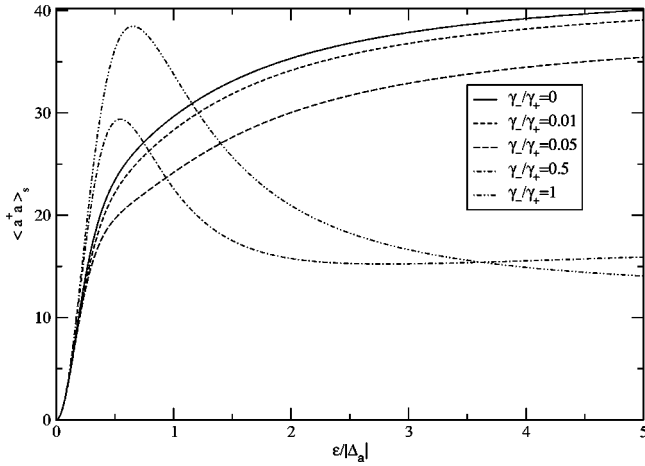


FIG. 11. The steady-state mean number of photons in the cavity $\langle a^\dagger a \rangle_s$ in the presence of dipolar dephasing, as a function of the scaled driving field Rabi frequency $\varepsilon/|\Delta_a|$, for negative detuning between the atomic resonant frequency and the driving field frequency $\Delta_a < 0$, and for various values of the jump in the photonic DOS γ_-/γ_+ . We have set $\kappa = 0.1\gamma_+$, $g = 10\kappa$, and $\gamma_p = 0.1\gamma_+$ in the calculations.

$\langle a \rangle_s$. For small values of $\langle R_3 \rangle_s$, the source term in Eq. (4.1a) is very small, and the field amplitude decreases in time and reaches a very small steady-state value (equal to zero in the case of free space, where $\langle R_3 \rangle_s = 0$).

We now investigate the effect of additional dephasing on the emission characteristics. In Fig. 11, we plot the steady-state mean number of photons in the cavity field as a function of the pump intensity, when additional dephasing is present in the system. Clearly, the dephasing processes suppress the emission process, lowering the number of photons in the cavity mode, relative to the case when no dipolar dephasing is present (see Fig. 9). This deleterious effect on the light generation is more pronounced in photonic structures presenting large jumps in the photonic DOS. We also obtain that, although the emission is enhanced for large jumps in the photonic DOS at large values of the driving field intensity, the number of photons in the cavity field in this case is comparable to that obtained in free space for smaller values of the pumping field intensity. However, better coherence of the cavity field may be achieved in photonic crystals, as we show in Sec. V.

In Fig. 12, we plot the mean number of photons in the cavity versus the scaled cavity decay rate, $\kappa/\gamma_+ = (\omega/\gamma)/(Q\gamma_+/\gamma)$, in the absence of dipolar dephasing, and for various jumps in the photonic DOS, for $\Delta_a < 0$, and $\varepsilon/|\Delta_a| = 2$. Clearly, the light emission is enhanced for larger jumps in the photonic density of states. Also, the mean number of photons in the cavity field increases with the cavity quality factor and the spontaneous emission decay ratio γ_+/γ . The effect of the additional dephasing on these features is investigated in Fig. 13. We note that the emission enhancement relative to free space for large jumps in the photonic density of states, although reduced by the dephasing processes, is still preserved for high- Q -factor microcavities.

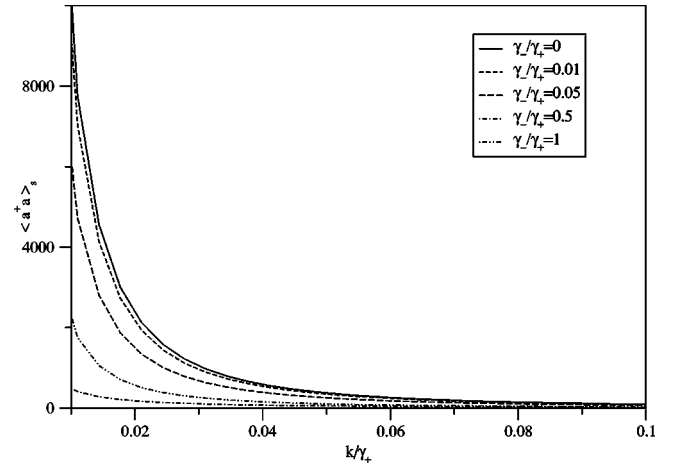


FIG. 12. The steady-state mean number of photons in the cavity $\langle a^\dagger a \rangle_s$ as a function of the scaled cavity decay rate κ/γ_+ in the absence of dipolar dephasing, for negative detuning between the atomic resonant frequency and the driving field frequency $\Delta_a < 0$, and for various values of the magnitude of the jump in the photonic density of states γ_-/γ_+ . We have set $\varepsilon/|\Delta_a| = 2$, $g = \gamma_+$, and $\gamma_p = 0$ in the calculations.

V. PHOTON STATISTICS

In this section, we analyze the coherence properties of the light emitted into the cavity mode of our one-atom PBG microchip laser, using the quantum degree of second-order coherence, $g^{(2)}(0)$. This one-time normalized second-order correlation function, defined as

$$g^{(2)}(0) = \frac{\langle a^{\dagger 2} a^2 \rangle_s}{\langle a^\dagger a \rangle_s^2}, \quad (5.1)$$

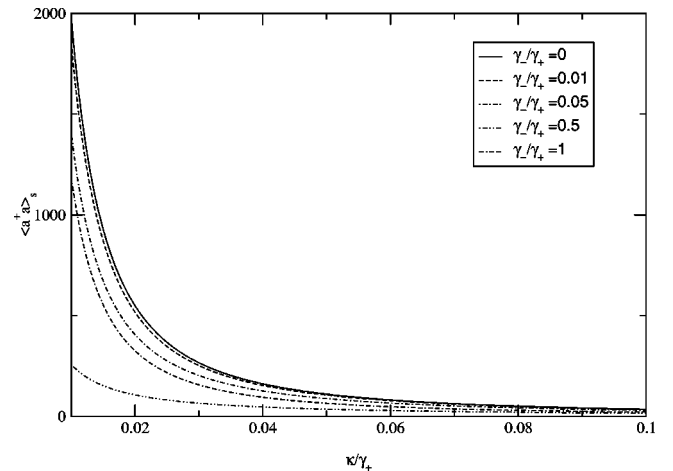


FIG. 13. The steady-state mean number of photons in the cavity $\langle a^\dagger a \rangle_s$ in the presence of dipolar dephasing, as a function of the scaled cavity decay rate κ/γ_+ for negative detuning between the atomic resonant frequency and the driving field frequency $\Delta_a < 0$, and for various values of the magnitude of the jump in the photonic density of states γ_-/γ_+ . We have set $\varepsilon/|\Delta_a| = 2$, $g = \gamma_+$, and $\gamma_p = 0.1\gamma_+$ in the calculations.

can distinguish laser light from the chaotic light generated from a thermal source. For chaotic light $g^{(2)}(0)=2$, while $g^{(2)}(0)=1$ for a source of coherent light [31,16].

Generally, the moments in the definition (5.1) of the quantum degree of second-order coherence may be calculated by numerical means, using the solution of the master equation (3.16), or approximately, by means of certain factorization schemes. However, our model enables an exact and simple analytical solution for the emitted photon statistics. The following equations of motion can be derived from the master equation (3.16):

$$\frac{d}{dt}\langle a^{+2}a^2 \rangle = -2\kappa\langle a^{+2}a^2 \rangle + 2g_1\langle a^{+2}aR_3 \rangle + 2g_1\langle a^\dagger a^2 R_3 \rangle, \quad (5.2a)$$

$$\begin{aligned} \frac{d}{dt}\langle a^{+2}aR_3 \rangle &= -(\gamma_1 + 3\kappa/2)\langle a^{+2}aR_3 \rangle + g_1\langle a^{+2} \rangle \\ &\quad + 2g_1\langle a^\dagger a \rangle - \gamma_2\langle a^{+2}a \rangle, \end{aligned} \quad (5.2b)$$

$$\frac{d}{dt}\langle a^{+2} \rangle = -\kappa\langle a^{+2} \rangle + 2g_1\langle a^\dagger R_3 \rangle, \quad (5.2c)$$

$$\frac{d}{dt}\langle a^{+2}a \rangle = -3(\kappa/2)\langle a^{+2}a \rangle + 2g_1\langle a^\dagger aR_3 \rangle + g_1\langle a^{+2}R_3 \rangle, \quad (5.2d)$$

$$\frac{d}{dt}\langle a^{+2}R_3 \rangle = -(\gamma_1 + \kappa)\langle a^{+2}R_3 \rangle + 2g_1\langle a^\dagger \rangle - \gamma_2\langle a^{+2} \rangle, \quad (5.2e)$$

$$\begin{aligned} \frac{d}{dt}\langle a^\dagger aR_3 \rangle &= -(\gamma_1 + \kappa)\langle a^\dagger aR_3 \rangle + g_1(\langle a \rangle + \langle a^\dagger \rangle) \\ &\quad - \gamma_2\langle a^\dagger a \rangle. \end{aligned} \quad (5.2f)$$

In steady state, Eqs. (5.2) together with Eqs. (4.1) constitute a closed linear system of equations. Their solution gives the quantum degree of second-order coherence:

$$g^{(2)}(0) = 1 + (\gamma_1^2 - \gamma_2^2) \frac{4\kappa(4\gamma_2^2\gamma_1 + 3\gamma_2^2\kappa + \gamma_1\kappa^2 + \kappa\gamma_1^2)}{(\kappa\gamma_1 + 2\gamma_2^2)^2(\kappa + \gamma_1)(3\kappa + 2\gamma_1)}, \quad (5.3)$$

$g^{(2)}(0)$ depends implicitly on the pump intensity through $\gamma_{1,2}$. We first note that, in general, the emitted field photon statistics is super-Poissonian, $g^{(2)}(0) > 1$. This is a direct consequence of the fact that $\gamma_1^2 \geq \gamma_2^2$. In the case of vanishing mode density on the lower Mollow sideband ($\gamma_- = 0$) and no dipolar dephasing ($\gamma_p = 0$), $\gamma_1 = \gamma_2$ [see the definition (4.2) for $\gamma_{1,2}$], and the cavity field photon statistics is Poissonian. Physically, the enhancement of coherence for larger jump in the photonic density of modes arises because the bare atomic system becomes inverted [26] (see also Fig. 10). In this case, the system is similar to a conventional laser operating well above the threshold.

From the analytical expression (5.3), it follows that the quantum degree of second-order coherence of the cavity field

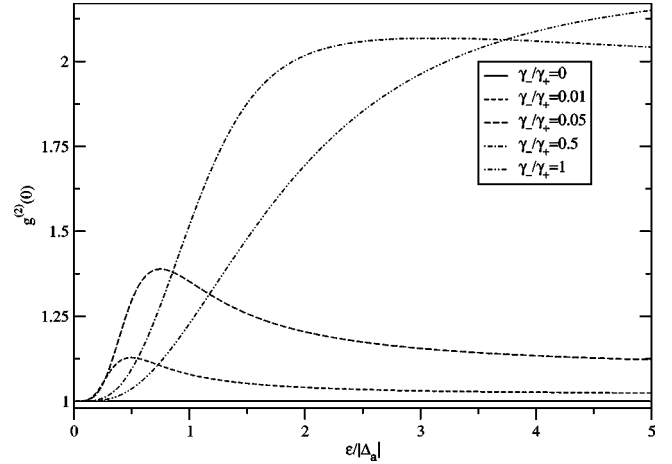


FIG. 14. The quantum degree of second-order coherence, $g^{(2)}(0)$, as a function of the scaled driving field Rabi frequency $\varepsilon/|\Delta_a|$, for the case when no dipolar dephasing is present in the system, for negative detuning between the atomic resonant frequency and the driving field frequency, and for various values of the jump in the photonic density of states γ_-/γ_+ . We have set $\kappa = 0.1\gamma_+$, $g = 10\kappa$, and $\gamma_p = 0$ in the calculations.

exhibits a local maximum as a function of the intensity of the driving field. This maximum occurs when $\tan^4(\phi) = \gamma_+/\gamma_-$ ($\gamma_2 = 0$) and corresponds physically to the pump intensity that causes the bare atomic inversion [see Eqs. (3.11b) and (4.3)]. In addition, one can show (see the Appendix) that at this inversion threshold only the even moments of the photon distribution $\langle a^{2n} \rangle_s$ are nonzero, while all odd moments $\langle a^{2n+1} \rangle_s$ vanish. Physically, this local maximum in the second-order coherence function corresponds to the tendency of emitting photons in pairs (photon bunching).

In Fig. 14, we plot the quantum degree of second-order coherence, $g^{(2)}(0)$, as a function of Rabi driving field frequency ε , in the case when no dipolar dephasing is present in the system, and for the same values of the parameters γ_-/γ_+ , Δ_a , κ , and g as for Fig. 9. For small values of the driving field intensity, the quantum degree of second-order coherence increases with the magnitude of the radiation reservoir photonic DOS discontinuity, and, in fact, better coherence occurs in free space. However, we note from Fig. 9 that the mean photon number in this case is small. For larger values of the driving field intensity (when the mean number of photons is large), $g^{(2)}(0)$ decreases with the magnitude of the discontinuity in the photonic DOS. Moreover, $g^{(2)}(0)$ tends to 1, as it does for coherent states, in the limit of zero mode density on the lower Mollow sideband. Dipolar dephasing reduces the coherence of the cavity field, as shown in Fig. 15, where we plot $g^{(2)}(0)$ as a function of the pump field intensity for $\gamma_p \neq 0$. We find that better coherence is obtained, once again, for large values of the discontinuity in the photonic DOS.

In Fig. 16, we study $g^{(2)}(0)$ as a function of the scaled cavity decay rate κ/γ_+ for the same parameters γ_-/γ_+ , Δ_a , $\varepsilon/|\Delta_a|$, and g , as those used for Fig. 12. For all values of the cavity decay rate, the photon statistics of the cavity field is more Poissonian (coherent light) for larger disconti-

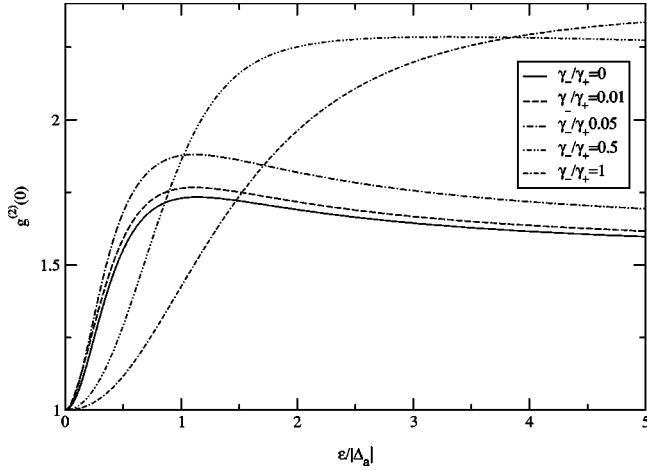


FIG. 15. The quantum degree of second-order coherence, $g^{(2)}(0)$, as a function of the scaled driving field Rabi frequency $\varepsilon/|\Delta_a|$, in the presence of dipolar dephasing, for negative detuning between the atomic resonant frequency and the driving field frequency, and for various values of the jump in the photonic density of states γ_-/γ_+ . We have set $\kappa=0.1\gamma_+$, $g=10\kappa$, and $\gamma_p=0.1\gamma_+$ in the calculations.

nities in the photonic DOS. Also, we note that in the limit of large cavity decay rate, the emission becomes Poissonian, irrespective of the properties of the density of states of the photonic reservoir. However, in this case, the number of photons in the cavity field is very small (see Fig. 12). The influence of the dipolar dephasing on these characteristics is presented in Fig. 17, where we plot $g^{(2)}(0)$, as a function of the scaled cavity decay rate κ/γ_+ for the same parameters γ_-/γ_+ , Δ_a , $\varepsilon/|\Delta_a|$, and g , as those used for Fig. 16 and for $\gamma_p=0.1\gamma_+$. We obtain a loss of coherence for all values of the cavity decay rate, relative to the case when no dipolar dephasing is present in the system.

In the following, we investigate the quadrature coherence of the cavity field, by analyzing the variances of the conju-

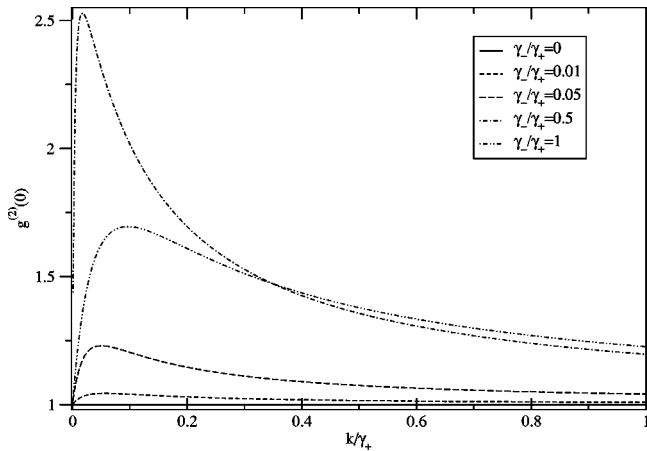


FIG. 16. The quantum degree of second-order coherence, $g^{(2)}(0)$, as a function of the scaled cavity decay rate κ/γ_+ , in the absence of dipolar dephasing, for negative detuning between the atomic resonant frequency and the driving field frequency $\Delta_a < 0$, and for various values of the jump in the photonic density of states γ_-/γ_+ . We have set $\varepsilon/|\Delta_a|=2$ and $g=\gamma_+$ in the calculations.

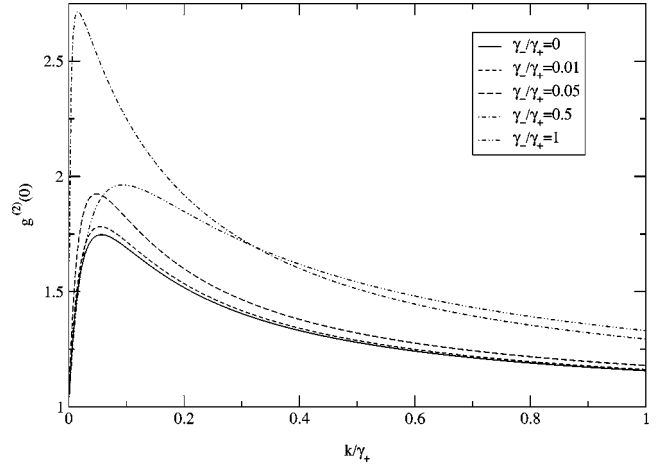


FIG. 17. The quantum degree of second-order coherence, $g^{(2)}(0)$, as a function of the scaled cavity decay rate κ/γ_+ , in the presence of dipolar dephasing, for negative detuning between the atomic resonant frequency and the driving field frequency $\Delta_a < 0$, and for various values of the jump in the photonic density of states γ_-/γ_+ . We have set $\varepsilon/|\Delta_a|=2$, $g=\gamma_+$, and $\gamma_p=0.1\gamma_+$ in the calculations.

gate quadratures $X_+=[a^\dagger+a]/2$ and $X_-=[a^\dagger-a]/2i$. Using the solution of Eqs. (4.1a)–(4.1c) and (5.2), we obtain

$$\langle(\Delta X_+)^2\rangle_s = \frac{1}{4} + (\gamma_1^2 - \gamma_2^2) \frac{4g_1^2}{\kappa\gamma_1(\kappa + 2\gamma_1)} \quad (5.4)$$

and

$$\langle(\Delta X_-)^2\rangle_s = \frac{1}{4}. \quad (5.5)$$

Clearly, from Eq. (5.5), the variance of one of the quadratures is independent of the properties of the photonic reservoir and the cavity decay, and it reaches the level of the quantum shot noise limit. In the case of emission in a full photonic band gap and no dipolar dephasing ($\gamma_1=\gamma_2$), the variances of both conjugate quadratures are characterized by the quantum shot noise limit. That is, the cavity field is characterized by quadrature coherence.

VI. CONCLUSIONS

We studied the emission properties, photon statistics, and quadrature coherence properties of a one-atom laser with coherent pumping in photonic crystals. We considered the case when the cavity frequency is tuned close to the Mollow central component. In the limit of strong pumping, we derived analytical expressions for the amplitude, mean photon number, quantum degree of second-order coherence, and high-order moments of the cavity field. We showed that, for a photonic density of states of the photonic radiation reservoir presenting a discontinuity, the fluorescent intensity emerging from the cavity is strongly enhanced and more coherent relative to the corresponding cavity in a free-space reservoir. The variance of one of the quadratures is characterized by the quantum shot noise limit, independently of the photonic res-

ervoir and the cavity decay. If the microcavity resonance occurs in a full photonic band gap ($\gamma_1 = \gamma_2$), the variance of both conjugate quadratures is characterized by the quantum shot noise limit. Physically, this could be realized in a single-mode waveguide channel in a PBG. Also, under certain conditions, only the even moments $\langle a^{2n} \rangle$ can be nonzero, while the odd moments $\langle a^{2n+1} \rangle$ are equal to zero. This suggests that only the even off-diagonal density matrix elements $\rho_{m,m\pm 2n}^{(c)}$ are nonzero.

Our study corresponds to the case when the atomic system is pumped by a strong coherent laser field. In the context of a submicrometer scale waveguide channel in a PBG, strong fields can be realized with very low pump power on the scale of nanowatts. By using a strong laser field, it is possible to drive the Mollow spectral components of resonance fluorescence away from the singularity of the photon density of states, such that over the width of the individual sidebands the density of states is smooth. It would be of considerable interest to extend this model to include both weak and strong pumping fields. For weaker fields, the singularity in the photonic density of states at the photonic band edge may lead to non-Markovian effects in the atom–radiation reservoir interaction. In this case, the temporal evolution of the atom–photonic reservoir system requires that we generalize the equations of motion for the atomic variables to a set of integro-differential equations, appropriate for a photonic band-gap material. Given these clear distinguishable features resulting from photonic crystal architecture on one-atom properties, it is likely that even more dramatic effects will be observed for a large collection of N atoms (quantum dots) placed within the dielectric defect. Our results clearly illustrate the ability to “engineer” quantum optical characteristics in coherent atom–radiation interactions through suitable photonic crystal architectures.

APPENDIX: HIGH-ORDER MOMENTS

In Sec. III we derived the expression for the steady-state amplitude of the cavity field $\langle a \rangle_s$. We note that in certain

cases it vanishes, while the intensity of the cavity field, $\langle a^\dagger a \rangle_s$ may be very large for the strong coupling limit. In this section, we discuss the high-order moments $\langle a^n \rangle_s$ and associated off-diagonal cavity density matrix elements $\rho_{m,m+n}^{(c)}$ for these cases. The following equations of motion can be derived from the master equation (3.16):

$$\frac{d}{dt} \langle a^n \rangle = -n \left(\frac{\kappa}{2} \right) \langle a^n \rangle + g_1 n \langle a^{n-1} R_3 \rangle, \quad (\text{A1})$$

$$\frac{d}{dt} \langle a^m R_3 \rangle = - \left[\gamma_1 + m \left(\frac{\kappa}{2} \right) \right] \langle a^m R_3 \rangle + m g_1 \langle a^{m-1} \rangle - \gamma_2 \langle a^m \rangle. \quad (\text{A2})$$

At the bare atomic population inversion threshold, $\gamma_2 = 0$. In this case, the relation between steady-state values $\langle a^n \rangle_s$ and $\langle a^{n-2} \rangle_s$ is found from Eqs. (A1) and (A2) as

$$\langle a^n \rangle_s = \frac{2g_1^2}{\kappa} \frac{(n-1) \langle a^{n-2} \rangle_s}{2\gamma_1 + (n-1)\kappa}. \quad (\text{A3})$$

Here, for simplicity, we have considered the cavity frequency tuned to resonance with the driving field frequency.

Using Eqs. (A2) and (3.6), we can find $\langle a^n \rangle_s$ as

$$\langle a^{2n} \rangle_s = \langle a^{+2n} \rangle_s = \frac{g_1^{2n}}{\kappa^n} \prod_{m=1}^n \frac{2m-1}{\gamma_1 + (2m-1)\kappa}, \quad (\text{A4})$$

$$\langle a^{2n+1} \rangle_s = \langle a^{+2n+1} \rangle_s = 0. \quad (\text{A5})$$

Clearly, only the even moments $\langle a^{2n} \rangle_s$ are nonzero, while the odd moments $\langle a^{2n+1} \rangle_s$ vanish. This suggests that the density matrix of the cavity field $\rho^{(c)}$ has only nonzero elements $\rho_{m,m\pm 2n}^{(c)}$ ($2n < m$).

-
- [1] S. John, *Phys. Rev. Lett.* **53**, 2169 (1984).
 [2] E. Yablonovitch, *Phys. Rev. Lett.* **58**, 2059 (1987).
 [3] S. John, *Phys. Rev. Lett.* **58**, 2486 (1987).
 [4] S. John and J. Wang, *Phys. Rev. Lett.* **64**, 2418 (1990).
 [5] S. John and Tran Quang, *Phys. Rev. A* **50**, 1764 (1994).
 [6] S. John and Tran Quang, *Phys. Rev. Lett.* **78**, 1888 (1997); S. John and M. Florescu, *J. Opt. A, Pure Appl. Opt.* **3**, S103 (2001).
 [7] C.M. Cornelius and J.P. Dowling, *Phys. Rev. A* **59**, 4736 (1999); J.G. Fleming, S.Y. Lin, I. Al-Kady, and K.M. Ho, *Nature (London)* **417**, 52 (2002).
 [8] Tran Quang, M. Woldeyohannes, S. John, and G.S. Agarwal, *Phys. Rev. Lett.* **79**, 5238 (1997); S.Y. Zhu, H. Chen, and Hu Huang, *ibid.* **79**, 205 (1997); D.G. Angelakis, E. Paspalakis, and P.L. Knight, *Phys. Rev. A* **64**, 013801 (2001); Y.V. Rostovtsev, A.B. Matsko, and M.O. Scully, *ibid.* **57**, 4919 (1998).
 [9] *Photonic Band Gap Materials*, Vol. 315 of *NATO Advanced Study Institute, Series E: Applied Physics*, edited by C.M. Soukoulis (Kluwer Academic, Dordrecht, 1996); *Photonic Crystals and Light Localization in the 21st Century*, Vol. 563 of *NATO Advanced Study Institute, Series C: Mathematical and Physical Sciences*, edited by C.M. Soukoulis (Kluwer Academic, Dordrecht, 2001).
 [10] M. Loncar, T. Yoshie, A. Scherer, P. Gogna, and Y. Qiu, *Appl. Phys. Lett.* **81**, 2680 (2002); M. Loncar, A. Scherer, and Y. Qiu, *ibid.* **82**, 4648 (2003); M. Imada, S. Noda, A. Chutinan, T. Tokuda, M. Murata, and G. Sasaki, *ibid.* **75**, 316 (1999); S. Noda *et al.* *Science* **293**, 1123 (2001); S. Noda, A. Chutinan, and M. Imada, *Nature (London)* **407**, 608 (2000).
 [11] M.G. Raizen, R.J. Thompson, R.J. Brecha, H.J. Kimble, and H.J. Carmichael, *Phys. Rev. Lett.* **63**, 240 (1989).
 [12] G. Rempe, R.J. Thompson, R.J. Brecha, W.D. Lee, and H.J. Kimble, *Phys. Rev. Lett.* **67**, 1727 (1991).
 [13] Q. A. Turchette, C. M. Hood, W. Lange, H. Mabuchi, and H. J.

- Kimble, Phys. Rev. Lett. **75**, 4710 (1995).
- [14] K. An, J.J. Childs, R.R. Dasari, and M.S. Feld, Phys. Rev. Lett. **73**, 3375 (1994).
- [15] M. Sargent, M. O. Scully, and W. E. Lamb, *Laser Physics* (Addison-Wesley, Reading, MA, 1974).
- [16] H. Haken, in *Light and Matter*, edited by L. Genzen, Vol. XXV/2c of *Handbuch der Physik* (Springer-Verlag, Berlin, 1970).
- [17] Y. Mu and C.M. Savage, Phys. Rev. A **46**, 5944 (1992).
- [18] Tran Quang and H. Freedhoff, Phys. Rev. A **47**, 2285 (1993); H. Freedhoff and Tran Quang, Phys. Rev. Lett. **72**, 474 (1994).
- [19] Young-Tak Chough, Hee-Jong Moon, Hyunchul Nha, and Kyungwon An, Phys. Rev. A **63**, 013804 (2000).
- [20] G.S. Agarwal, L.M. Narducci, Da Hsuan Feng, and R. Gilmore, Phys. Rev. Lett. **42**, 1260 (1978).
- [21] A. Chutinan, S. John, and O. Toader, Phys. Rev. Lett. **90**, 123901 (2003).
- [22] K.M. Leung and Y.F. Liu, Phys. Rev. Lett. **65**, 2646 (1990).
- [23] E. Yablonovitch, T.J. Gmitter, R.D. Meade, A.M. Rappe, K.D. Brommer, and J.D. Joannopoulos, Phys. Rev. Lett. **67**, 3380 (1991).
- [24] R.D. Meade, A. Devenyi, J.D. Joannopoulos, O.L. Alerhand, D.A. Smith, and K. Kash, J. Appl. Phys. **75**, 4753 (1994).
- [25] R.D. Meade, K.D. Brommer, A.M. Rappe, and J.D. Joannopoulos, Phys. Rev. B **44**, 13 772 (1991).
- [26] M. Florescu and S. John, Phys. Rev. A **64**, 033801 (2001).
- [27] A. E. Siegman, *Lasers* (University Science Books, Sausalito, CA, 1986).
- [28] O. Painter *et al.* Science **284**, 1819 (1999).
- [29] H. J. Carmichael, *Statistical Methods in Quantum Optics I* (Springer-Verlag, Berlin, 1999).
- [30] The intensity of an electromagnetic wave is the time average over the detector response time of the Poynting vector, describing the rate of flow of electromagnetic energy. For a plane wave, the intensity I and amplitude E of the electric field are related to each other by $I(\text{W/m}^2) \approx 1.33 \times 10^{-3} |E(\text{V/m})|^2$. Thus, an electric field amplitude $E \approx 10^3$ V/m gives an intensity $I \approx 10^3$ W/m². For a waveguide channel with cross-sectional area on the scale of $(\mu\text{m})^2$, this corresponds to a net power of about 1 nW.
- [31] R. Loudon, *The Quantum Theory of Light* (Oxford University Press, Oxford, 2002).